



# Cooperative Drone Delivery via Push-based Lift with Payload Stabilization

Alice James<sup>1</sup>, Avishkar Seth<sup>1</sup>, Endowednes Kuantama<sup>2</sup>, Richard Han<sup>2</sup>, Subhas Mukhopadhyay<sup>1</sup>

School of Engineering<sup>1</sup>, School of Computing<sup>2</sup>

Macquarie University, Australia

alice.james@mq.edu.au, avishkar.seth@mq.edu.au, endowednes.kuantama@mq.edu.au, richard.han@mq.edu.au, subhas.mukhopadhyay@mq.edu.au

## ABSTRACT

Advancements in robotics have led to innovative approaches that employ quadcopters for carrying loads. In this paper, we introduce a unique system: a cooperative aerial robot delivery system employing a push-based method to transport payloads. This system includes a self-stabilizing tray with dual resistive sensor panels and a highly responsive 3-degree end-effector servo control designed to counteract payload instability. In our experiments, two Unmanned Aerial Vehicles (UAVs) successfully transported three distinct payload types, varying in size, mainly under indoor conditions. The Self Balancing Tray's (SBT) servo angles demonstrated reliable precision, with deviations reaching 1.6% from the average, enabling a rapid transport speed of up to 4 meters per second. Such accuracy is vital for safely moving delicate payloads. During flight, the system adeptly adjusted the payload's position, requiring merely 2.4 seconds for re-stabilization. Furthermore, the 3-degree end-effector (3-DEE) significantly minimized vibrations, enhancing the system's stability. These findings demonstrate the feasibility of push-based lift for cooperative drone payload transport systems.

## CCS CONCEPTS

- Computer systems organization → Robotics; • Applied computing → Aerospace.

## KEYWORDS

Drone, UAV, Swarm, Delivery, Cooperative

## ACM Reference Format:

Alice James<sup>1</sup>, Avishkar Seth<sup>1</sup>, Endowednes Kuantama<sup>2</sup>, Richard Han<sup>2</sup>, Subhas Mukhopadhyay<sup>1</sup>. 2024. Cooperative Drone Delivery via Push-based Lift with Payload Stabilization. In *The 10th Workshop on Micro Aerial Vehicle Networks, Systems, and Applications (DroNet' 24)*, June 3–7, 2024, Minato-ku, Tokyo, Japan. ACM, New York, NY, USA, 6 pages. <https://doi.org/10.1145/3661810.3663468>

## 1 INTRODUCTION

The field of aerial robotics has grown enormously in the past decade, with advances in computation, flight control systems, and sensor technology. Unmanned Aerial Vehicles (UAVs), particularly quadcopters, have emerged as pivotal platforms owing to their Vertical

Takeoff and Landing (VTOL) capabilities. This versatility has propelled advancements in aerial manipulation [25, 26], swarm capabilities [2, 3, 27], transporting objects [8, 13, 22] and bio-inspired UAVs [6, 10, 16].

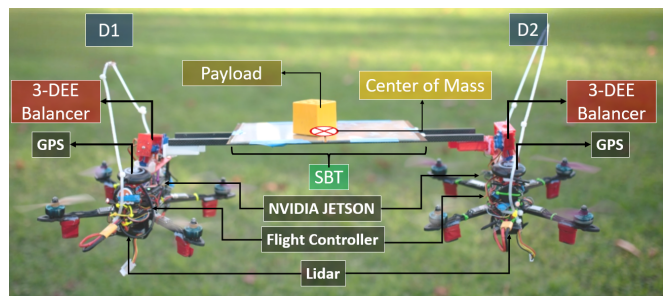


**Figure 1: The Cooperative Aerial Robots Push-based Lift System in flight with major components labelled**

Drones are typically designed for different payload capacities, and the total thrust limitations of individual drones restrict the payload they can lift. Using larger drones to carry high-capacity payloads can be unsafe for people and become too expensive and bulky, thus reducing their stability [19]. In the case of novel methods of single drone payload lifts, using a reconfigurable multirotor design [18], adding additional safety features [13], or placing payloads above the UAV [12, 21] has been explored. In practice, adding additional hardware attachments to the UAVs can cause instability, control complexities, and require appropriate dynamic tuning while managing their CoG (Center of Gravity) [14].

Using multiple cooperative aerial robots to manipulate and carry single larger payloads is gaining traction. Multiple UAVs have various methods of jointly lifting a load, similar to the challenge of attaching payloads to a single drone with different aerial system configurations [1]. Experimental systems for cooperative transport using drones, typically employing two to four drones, have commonly implemented a lift or pull-based method, positioning the drones above or beside the load being transported, as exemplified in studies by recent researchers [5, 17, 23, 24]. These pull-based paradigms all exhibit similar disadvantages, namely, the payload underneath the drones is subject to strong downwash from the drone propellers, typically inducing a pendulum swing that can further disbalance the payload, causing additional strain on the cooperative drones, potentially damaging the payload, and inducing intense vibrations on the drone.

In contrast, we present a new cooperative drone payload delivery system with a self-balancing tray (SBT) strategically mounted above



This work is licensed under a Creative Commons Attribution-NonCommercial-ShareAlike International 4.0 License.

*DroNet' 24*, June 3–7, 2024, Minato-ku, Tokyo, Japan

© 2024 Copyright held by the owner/author(s).

ACM ISBN 979-8-4007-0656-1/24/06.

<https://doi.org/10.1145/3661810.3663468>

the drones, as shown in Fig. 1. The drones lift the tray using a "push" mechanism, which helps avoid the instability commonly seen with sling-/pull-based lifting methods. To maintain balance, the tray has a distributed 3-degree end effector (3-DEE) servomotor control system. This innovative approach facilitates flexible and synchronized collaboration between the two drones, showcasing the system's ability to keep the centre of mass stable during flight. The key contributions of this study include:

- Introduction of a novel concept of a flexible push-based cooperative lift, where two drones push a tray carrying items to be lifted and transported.
- A novel SBT with sensor fusion method to balance payloads of different sizes to maintain the system equilibrium during transport.
- Implementation of asynchronous angle adjustments between the two drones and the Self-Balancing Tray (SBT) that can sense and adjust the system's attitude based on individual drone movements, lowering vibrations compared to rigidly attached systems.

The paper is organized as follows: section 2 provides a literature overview, section 3 provides the system architecture, and section 4 presents the results, followed by the conclusion and future work.

## 2 RELATED WORK

The pull-based lift method using a suspended cable poses significant challenges in stability and control due to trajectory adjustments that may disrupt load balance, inducing swaying and wind disturbances and introducing load oscillations [4]. It is essential to consider these factors when implementing the pull-based method for optimal results [1, 20]. There may be slipstream issues in situations where larger objects are being transported, caused by interference from the downward force of the propeller [12, 21]. Some approaches incorporate robotic arms for more secure load grasping underneath [9], while others utilize electromagnets [15]. Alternatively, fixed and rigid attachments of drones to load and each other have been explored, forming a singular entity rather than an independently coordinated team of drones, restricting flexibility in supported load types [17, 24]. Furthermore, restricting flexibility disrupts flight dynamics, resulting in vibrations in the aircraft; in contrast, this research introduces the 3-DEE control for the SBT, which demonstrates smooth translation during transport. Computational Fluid Dynamics (CFD) is critical in drone aerodynamics, simulating airflow around the drone and propellers to precisely model aerodynamic forces such as lift, drag, and thrust, crucial for stability and maneuverability [7]. The impact of downwash resulting in payload disbalance has been investigated in recent research on multi-robot systems transporting payloads, which can be significant [4]. Extensive research has been conducted on aerodynamic analyses and disturbances for payload stability, particularly in delivery scenarios. However, such studies have been observed to focus mainly on hovering flight while not adequately addressing the complexities associated with cruise flight and real-world conditions [11–13]. Contrary to the previous work, this research demonstrates payload balance while the two drones move in translation. The payload's position relative to the drone's center of gravity critically impacts these dynamics. Payloads should be near the centre of gravity to

ensure balanced weight distribution and reduce thrust strain. This has been further elaborated in our preliminary work [21].

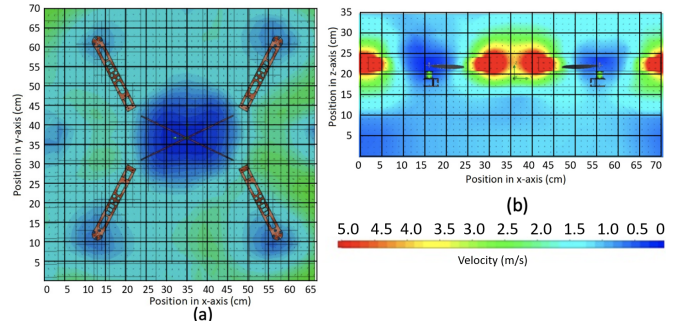


**Figure 2: CFD simulation images [21] of the UAV when a payload is placed below depicting a higher aerodynamic disturbance detected around the propellers (a) Bottom View (b) Side View**

In scenarios with excessive wind resistance, especially during translation, suspending the payload below using string or rigid attachments may cause turbulence due to the payload's position, potentially leading to instability. Fig. 2 shows the airflow around the propeller at a given velocity, showing how the propeller's rotation creates a relative aerodynamic disturbance by placing the payload below.

In summary, while existing research advances aerodynamics and drone design, it often overlooks the nuances of cruise flight and real-world applications. Our approach suggests a different perspective from the payload lifting approach that has the potential to improve existing systems.

## 3 SYSTEM OVERVIEW

### 3.1 Hardware Architecture

The system's architecture shown in Fig. 1 comprises two drones that connect to the Self Balancing Tray (SBT) using magnetic points in a push-based arrangement. These connections are designed for easy detachment, enabling compatibility with standard multirotors and potential scalability for more extensive collaborative tasks. Sensors embedded within the SBT monitor balance, while each drone is furnished with 3-degree end effector (3-DEE) actuators to balance the tray and uphold stability. The leading drone, D1, receives pressure data from the tray in a hierarchical configuration. It guides the follower drone D2 on adjustments while ensuring precise positioning using an NVIDIA Jetson Nano onboard computer (OBC) that communicates with the flight controller via MAVLINK and a ROS network partially adapted from prior work [22]. The flight controller interacts with flight controls, positioning sensors, and a resistive panel that assists in localising the payload. An Arduino Nano 33 IoT microcontroller oversees the SBT servo 3-DEE actuators, establishing bidirectional communication with the OBC. The operational protocol involves the leading drone providing the SBT with target GPS coordinates, which the follower drone verifies before commencing payload transportation. The drones, which

have been tested and are sized at 295mm, can accommodate varying payload weights and thrust capacities, utilising 3-blade 5-inch propellers with 1900 kV that can lift up to 2.5 kg.

### 3.2 3-DEE Model

The 3-DEE technique installed on each drone includes three servomotors - S1, S2 and S3. These motors are responsible for adjusting the pitch angles ( $\pm\phi$ ), roll ( $\pm\theta$ ) and yaw angles ( $\pm\psi$ ) of the drone SBT assembly with great precision. To maintain altitude, the drone uses an onboard LiDAR ranging sensor for essential system control, while the 3-DEE system offers accurate control over the payload. This ensures that the payload's center of gravity remains stable even as its position changes. The servo motors are controlled by the Arduino board, allowing for wireless position data transmission between the leader and follower drones via BLE. This ensures synchronised control of the SBT. The design of the drones is scalable for multi-drone operations and utilises magnets to attach them to the SBT.

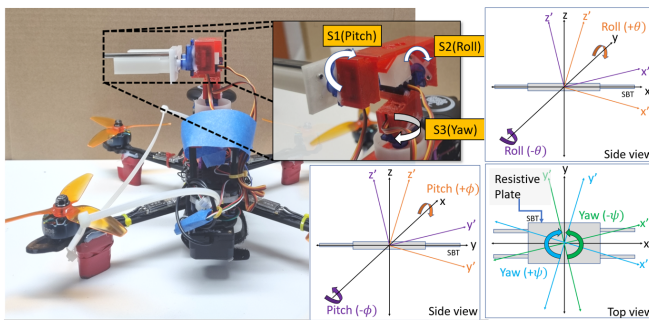


**Figure 3: The 3-DEE for SBT system showing the coordinates and motion capability**

In Fig. 3, various system parameters are depicted, facilitating the control of 3-DEE. Fig. 3 also illustrates the pitch, roll, and yaw coordinate reference frames, emphasising the SBT movement for the greatest deviation in all three axes. This frame of reference offers feedback on the regions experiencing maximum pressure at a specific time, allowing for estimating the SBT angle.

The precise shifting and positioning measurements of the payload are ensured by the resistive panels integrated into the tray in the SBT control system. These panels detect the contact locations in the X and Y directions using a gap between the conductive sheets. This facilitates accurate monitoring of the tray position and payload alignment. Each panel has dimensions of 1700 x 1300 mm, and it employs a grid system of blocks measuring 420 x 440 mm to represent payload positions. Feedback from the resistive panels guides the adjustment of the 3-DEE servo for pitch and roll movements. Specific grid points trigger horizontal movements for axis balancing. A heat map in Fig. 4 (a) aids in determining the SBT's centre coordinates and optimal adjustment zones by illustrating deviations in pitch and roll angles.

### 3.3 Dynamic Control

Dynamic control enables drones to maintain linear movement in the x and y directions by limiting the angle differences between drones

and the system base target (SBT). This approach incorporates a trajectory equation that accounts for the angles of the pitch ( $\phi$ ), roll ( $\theta$ ), and yaw ( $\psi$ ). We control the drone's rotational movements in the horizontal plane by converting angular body rates from  $[x \ y \ z]^T$  to Euler rates  $[\dot{\phi} \ \dot{\theta} \ \dot{\psi}]^T$  and using the angular velocity  $v$ , as detailed in the equation:

$$v = \begin{bmatrix} x \\ y \\ z \end{bmatrix} = \begin{bmatrix} 1 & 0 & -\sin\theta \\ 0 & \cos\phi & \sin\phi\cos\theta \\ 0 & -\sin\phi & \cos\phi\cos\theta \end{bmatrix} \begin{bmatrix} \dot{\phi} \\ \dot{\theta} \\ \dot{\psi} \end{bmatrix} \quad (1)$$

The gyroscope plays an essential role in gauging the angular velocities along the x, y, and z axes of the drone. Such measurements enable the assessment of angular displacement in the drone's body frame. Equation 2 facilitates the computation and monitoring of changes in angular positions during the drone's flight.

$$\begin{bmatrix} \dot{\phi} \\ \dot{\theta} \\ \dot{\psi} \end{bmatrix} = \begin{bmatrix} 1 & \sin\phi\tan\theta & \cos\phi\tan\theta \\ 0 & \cos\phi & -\sin\phi \\ 0 & \frac{\sin\phi}{\cos\theta} & \frac{\cos\phi}{\cos\theta} \end{bmatrix} \begin{bmatrix} x \\ y \\ z \end{bmatrix} \quad (2)$$

As indicated in Eq. 2, trigonometric functions determine positional and angular variations for each motion. This equation represents a 3x3 matrix corresponding to the axes (x, y, and z). Eqs. 1 and 2 emphasise the rotational dynamics of the quadcopter frame about each axis. We consider the coordinate frames for each drone. Fig. 3 shows the drone and SBT coordinate frames.  $[D1_x, D1_y, D1_z]$  and  $[D2_x, D2_y, D2_z]$  represent drones 1 and 2, respectively. The combined coordinate frame, which represents the overall system, is denoted as  $[Dt_x, Dt_y, Dt_z]$ . The net movement and direction of the drones are determined using the Euler formula. The overall dynamics of the system are represented by the sum of the transformations of two drones, as described:

$$D_{\text{total}}(t) = D_1(t) + D_2(t) \quad (3)$$

This equation establishes the net rotational angles for the swarm's movement, which is crucial for synchronised and stable flight without considering external disturbances. Where  $D_{\text{total}}(t)$  represents the combined resultant angles for the drones as indicated in Eq. 4. The individual rotational movements for each of the resultant pitch angles ( $\phi$ ), roll angles ( $\theta$ ), and yaw angles ( $\psi$ ) are derived from the summation of the angles from both drones.

$$Dt_{\text{total}}(t) = \phi_{\text{total}}(t)\theta_{\text{total}}(t)\psi_{\text{total}}(t) \quad (4)$$

Each drone's attitude determines its overall movement direction and position by utilising the Euler formula. Each drone has four rotors, and the combination of rotational speed, weight, and gravitational forces determines the resulting angles of Yaw, Pitch, and Roll movements (this calculation excludes any external disturbances).

$$Dt_{\text{total}}(t) = \begin{bmatrix} c\theta_{DT}c\psi_{DT} & c\theta_{DT}s\psi_{DT} & -s\theta_{DT} \\ s\psi_{DT}s\theta_{DT}c\psi_{DT} - c\theta_{DT}s\psi_{DT} & c\theta_{DT}c\psi_{DT} + s\phi_{DT}s\theta_{DT}s\psi_{DT} & s\phi_{DT}c\theta_{DT} \\ c\phi_{DT}s\theta_{DT}c\psi_{DT} + s\phi_{DT}s\psi_{DT} & s\theta_{DT}c\phi_{DT}c\psi_{DT} - s\phi_{DT}s\psi_{DT} & -s\phi_{DT}c\theta_{DT} \end{bmatrix} \quad (5)$$

Equation (5) denotes the resulting rotational angle from the swarm lift in the SBT. In this context, 'c' stands for the cosine of the angle, and 's' represents the sine.

## 4 RESULTS AND VALIDATION

### 4.1 SBT Payload Balance

We first analyzed how payload size affects 3-DEE mobility and load distribution across the SBT grid. A heatmap representing 3-DEE angle displacements across two 6x4 actuator grids on the SBT is featured in Fig. 4. Actuators in rows A and D control forward and backward movements, with rows B and C managing lateral roll movements. The color gradient from red to blue in the heatmap shows servo angle deviations. Red signifies a positive deflection up to 34 degrees, and blue indicates a negative deflection down to -29 degrees. The heatmap analysis under different payload conditions

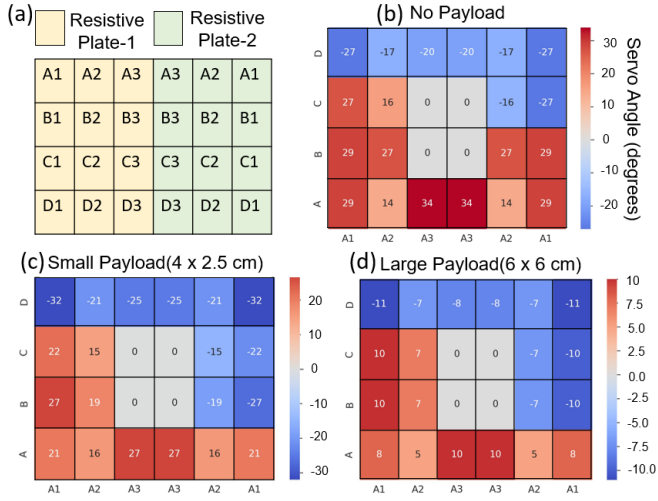


**Figure 4:** (a) Total drone coordinate frame for SBT resistive plates; SBT Movement angle deviation between 3-DEE Servo with two drones (b) no payload; (c) small payload (d) large payload

reveals distinct actuation patterns: In the no-payload condition, servo angles in row A range from 14 to 34 degrees, and in row D from -29 to -14 degrees, reflecting the maximal range without load. With a small payload (4x2.5 cm), the range narrows, with angles from 16 to 27 degrees in row A and -32 to -15 degrees in row D. Under a large payload (6x6 cm), the range reduces further to 5 to 10 degrees in row A and -11 to -7 degrees in row D, indicating significantly restricted actuator movement due to increased load.

This scenario vividly illustrates the substantially reduced actuator mobility due to the added load. Throughout the three conditions, the outermost grid positions (A1-A3 and D1-D3) maintain a broader range of motion than the central servos (B1-C3), illustrating a spatially-dependent load distribution. This differential load effect across the grid demonstrates the 3-DEE performance and ability with load variations.

We tested payloads on drones and measured their displacement offset from the centre of the SBT during flight. The 3-DEE system measured the payload position offset on the SBT during straight trajectory flights. We analyzed the average time as seen in Table 1 for the 3-DEE position correction system and heat maps of servo angle deviations to evaluate its efficiency under different payload

**Table 1: 3-DEE position correction performance**

Test case	Avg Pos. error (cm)	Avg Time
No-Payload	0.693	0.2 s
Small-Payload	1.107	1.9 s
Large-Payload	2.32	3.2 s

conditions. The system demonstrates superior precision for the no-payload scenario with an average positional error of just 0.693 cm and a swift average completion time of 0.2 seconds to correct the payload offset from the centre. The results indicate high control accuracy and responsiveness without additional weight. With the introduction of a small payload, positional error slightly increases to 1.107 cm, accompanied by a longer completion time of 1.9 seconds. This suggests a proportional relationship between payload size and control difficulty, with increased mass causing a modest drop in system precision and agility.

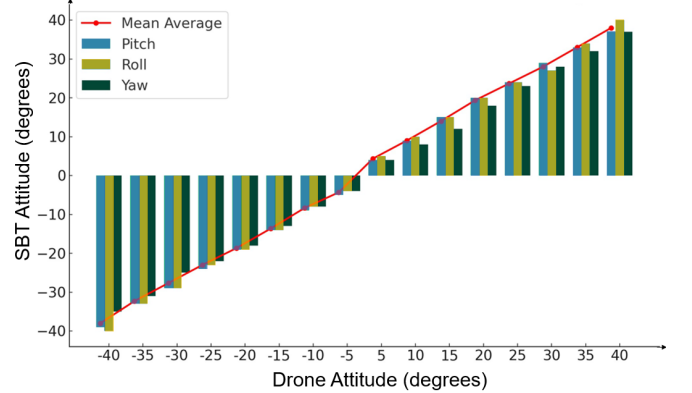


**Figure 5: Reliability Results of SBT angle in reference to the two drones**

The large payload condition further underscores this relationship, with the average positional error expanding to 2.32 cm and the completion time extending to 3.2 seconds. The heat maps and tabulated data collectively suggest that the adaptive SBT control system maintains payload centring with high accuracy. In the depicted Fig. 5 bar graph, we present the movement characteristics of a drone quantified in degrees, segregated into pitch, roll, and yaw across various positions. The bars indicate the individual degrees for pitch (blue), roll (yellow), and yaw (green) at drone positions ranging from -40 to 40. Overlaid is a mean average line (red), illustrating the central tendency of movement across the three examined axes.

Data reveals a linear relationship between drone positions and their angular movements across three dimensions, underscoring high stability and precise control. Numerically, the SBT's pitch, roll, and yaw are tightly clustered around -19, -19, and -18 degrees respectively when the drone's attitude is at -20 degrees. This indicates a control system precision within approximately 1.6% of the mean value, vital for precision-demanding tasks. Furthermore, centre of

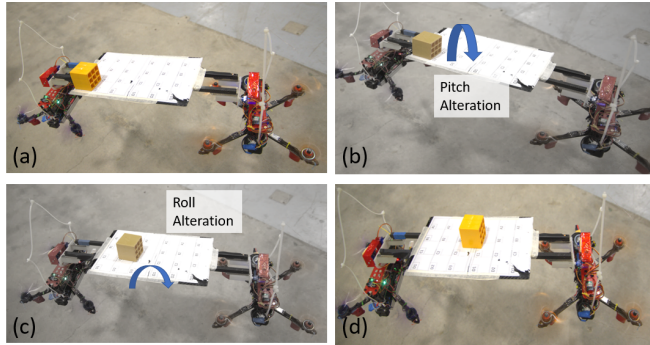


**Figure 6: Payload balancing(a) payload at extreme position (b) first-stage balance in pitch movement by SBT (c) second-stage balance in roll movement by SBT (d) payload adjusted back aligned in centre**

mass imbalances are corrected swiftly using SBT feedback to recenter the payload, enhancing stability. We observed that initially, the load was at the end of the pitch and roll movement, which would cause destabilization, and using the SBT feedback to resolve the balance of the bottle and the drones. For instance, feedback-driven adjustments allowed the SBT to stabilize the payload's shift within 2.4 seconds during flight, as shown in Fig. 6 and validated through camera observations.

## 4.2 Dynamic Push-lift Stabilization

We conducted experiments to assess the precision of the 3-DEE system to ensure the cooperative drones (D1 and D2) fly with the same attitude. During flight tests, the two drones have different attitudes while navigating a straight path, where D1's pitch or roll was defined, and then we observe D2 converge to the same attitude during flight. In the 3D line plot presented in Fig. 7, we observe the

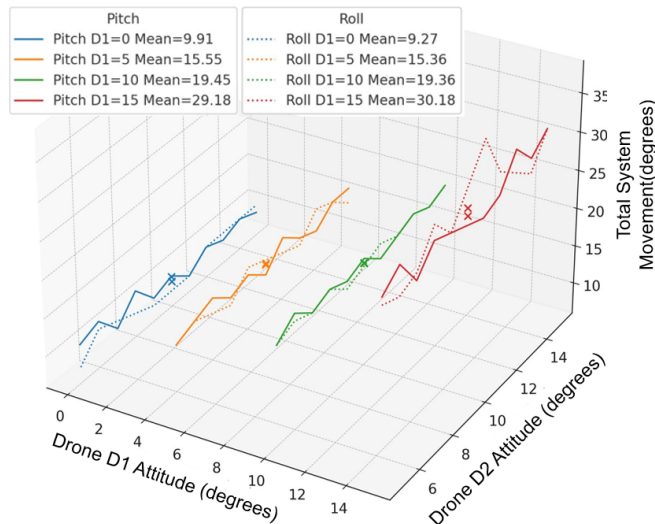


**Figure 7: Motion results for single drone angle alteration**

average movement of the pitch and roll of a cooperative system for 20 iterations of flight tests, demonstrating synchronous adjustment for change in individual drone movements. Each trajectory, signified by a unique colour, illustrates the evolution of movement averages as D2's attitude increments while holding D1 at a constant. The solid lines trace the pitch, while the dotted lines represent the roll, facilitating a comparative analysis between the two types of movement.

For each fixed D1 attitude (0, 5, 10, 15), the mean average values for pitch and roll are depicted by 'x' markers. For instance, at a D1=10, the average pitch for the cooperative system is measured at 19.45°, demonstrating D2's pitch attitude at an average of 10°. This suggests a proportional relationship between the two drones (D1 and D2) attitude for pitch and roll movements, indicative of the 3-DEE system's responsive behaviour. Notably, the largest mean average for cooperative pitch is found at D1 = 15° with a value of 29.18 degrees, closely followed by the cooperative roll's mean average of 30.18 degrees, indicating that D2 also converges to D2 = 15° on an average for pitch and roll.

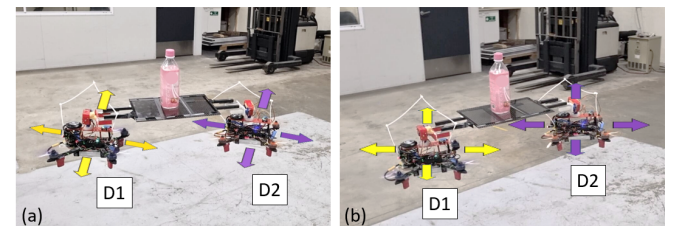


**Figure 8: Drone movement with a water bottle with a similar rotational angle.**

The data demonstrates that adjusting the drone's starting angle (D1) results in smooth pitch and roll movements, indicating a well-tuned system capable of stable payload control. Fig. 8 illustrates mid-flight coordination where both drones lift a partially filled bottle, maintaining identical rotational angles of 45 degrees in Fig. 8 (a) and 15 degrees in Fig. 8 (b). This synchronization ensures that both drones move in the same direction at a speed of 4 m/s, highlighting the system's effective control in maintaining coordinated drone movement and payload stability. The asynchronous angle behaviour can be observed in Fig. 8, showcasing the drones' response and adjustment to the asynchronous angles as observed in Fig. 7, highlighting how they adapt and maintain their flight characteristics despite the differing angles. Referencing the heatmap in Fig. 4, the SBT can balance the payload in the centre.

It is inadvisable to directly connect two drones without the 3-DEE system as it can lead to instability due to differences in response and vibrations, which may harm the payload's stability. An experiment was conducted to compare the effectiveness of a rigid body attachment without adaptive control (Fig. 9 (a)) to a servo-based adaptive control (Fig. 9 (b)), using fixed and 3-DEE-equipped attachments respectively. The experiment showed that the rigid body attachment produced excessive vibrations compared to the servo-based adaptive control, which used 3-DEE-equipped attachments. Vibration data from the MPU6000 sensor on the flight controller are within normal RMS thresholds:  $X \leq 2.2 \text{ m/s}^2$ ,  $Y \leq 2.8 \text{ m/s}^2$ ,  $Z \leq 2.8 \text{ m/s}^2$ ,

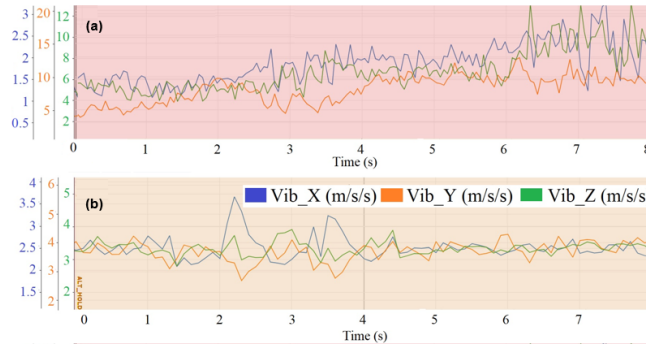


**Figure 9: The flight vibration results (a) rigidly attached payload, (b) payload with the 3 DEE.**

ensuring stable flight. The 3-DEE system implementation reduces vibrations, improving stability.

## 5 CONCLUSION

This study introduces a novel cooperative aerial robot system with a push-based lift and a 3-DEE servo manipulator linked to a Self-Balancing Tray (SBT), lifted by two drones. The system features a resistive sensing tray to adapt to shifting payloads. We tested the system with different payload sizes, using optical flow for indoor positioning and GPS outdoors. The results show average displacement offset from the centre of 0.693 cm, 1.107 cm, and 2.32 cm for no, small, and large payloads, demonstrating the system's adaptability. The SBT's servo angles ranging between  $34^\circ$  and  $-29^\circ$  had deviations within 1.6% of the mean, ensuring precise balance control and a speed of 4m/s. This accuracy is vital for sensitive payloads. The system quickly adjusts payload position, taking only 2.4 seconds to rebalance mid-flight. The 3-DEE position correction system also significantly reduced vibrations, enhancing stability. These findings demonstrate the feasibility of push-based lift for cooperative payload systems. Future work includes improving control stability and testing with various drones in diverse environments. We also will scale the system to accommodate configurations with multiple drones. Here is a video demonstration ([Link](#)).

## REFERENCES

- [1] Barakou, S.C., Tzafestas, C.S., Valavanis, K.P.: Real-time applicable cooperative aerial manipulation: A survey. In: 2023 International Conference on Unmanned Aircraft Systems (ICUAS). pp. 634–643 (2023). <https://doi.org/10.1109/ICUAS57906.2023.10155960>
- [2] Chung, S.J., Paranjape, A.A., Dames, P., Shen, S., Kumar, V.: A survey on aerial swarm robotics. IEEE Transactions on Robotics **34**(4), 837–855 (2018). <https://doi.org/10.1109/TRO.2018.285745>
- [3] Diller, J., Hall, P., Schenker, C., Ung, K., Belous, P., Russell, P., Han, Q.: Iccswarm: A framework for integrated communication and control in uav swarms. In: Proceedings of the Eighth Workshop on Micro Aerial Vehicle Networks, Systems, and Applications. p. 1–6. DroNet '22, Association for Computing Machinery, New York, NY, USA (2022). <https://doi.org/10.1145/3539493.3539579>
- [4] Estevez, J., Garate, G., Lopez-Guede, J.M., Larrea, M.: Review of aerial transportation of suspended-cable payloads with quadrotors. Drones **8**(2) (2024), <https://www.mdpi.com/2504-446X/8/2/35>
- [5] Gabrich, B., Saldaña, D., Kumar, V., Yim, M.: A flying gripper based on cuboid modular robots. In: 2018 IEEE International Conference on Robotics and Automation (ICRA). pp. 7024–7030 (2018). <https://doi.org/10.1109/ICRA.2018.8460682>
- [6] Goel, R., Pham, T., Nguyen, P., Hester, J.: Exploring batteryless uavs by mimicking bird flight. In: Proceedings of the Ninth Workshop on DroNet. p. 15–20. DroNet '23, ACM, New York, NY, USA (2023). <https://doi.org/10.1145/3597060.3597243>
- [7] Guo, Q., Zhu, Y., Tang, Y., Hou, C., He, Y., Zhuang, J., Zheng, Y., Luo, S.: Cfd simulation and experimental verification of the spatial and temporal distributions of the downwash airflow of a quad-rotor agricultural uav in hover. Computers and Electronics in Agriculture **172**, 105343 (2020). <https://doi.org/https://doi.org/10.1016/j.compag.2020.105343>
- [8] Kellermann, R., Biehle, T., Fischer, L.: Drones for parcel and passenger transportation: A literature review. Transportation Research Interdisciplinary Perspectives **4** (3 2020). <https://doi.org/10.1016/j.trip.2019.100088>
- [9] Kim, S., Seo, H., Shin, J., Kim, H.J.: Cooperative Aerial Manipulation Using Multi-rotors With Multi-DOF Robotic Arms. IEEE/ASME Transactions on Mechatronics **23**(2), 702–713 (2018). <https://doi.org/10.1109/TMECH.2018.2792318>
- [10] Kirchgeorg, S., Mintchev, S.: Hedgehog: Drone perching on tree branches with high-friction origami spines. IEEE Robotics and Automation Letters **7**(1), 602–609 (2022). <https://doi.org/10.1109/LRA.2021.3130378>
- [11] Kornatowski, P.M., Mintchev, S., Floreano, D.: An origami-inspired cargo drone. In: 2017 IEEE/RSJ International Conference on Intelligent Robots and Systems (IROS). pp. 6855–6862. IEEE/RSJ (2017). <https://doi.org/10.1109/IROS.2017.8206607>
- [12] Kornatowski, P.M., Feroskhan, M., Stewart, W.J., Floreano, D.: Downside up: rethinking parcel position for aerial delivery. IEEE Robotics and Automation Letters **5**(3), 4297–4304 (2020). <https://doi.org/10.1109/LRA.2020.2993768>
- [13] Kornatowski, P.M., Feroskhan, M., Stewart, W.J., Floreano, D.: A Morphing Cargo Drone for Safe Flight in Proximity of Humans. IEEE Robotics and Automation Letters **5**(3), 4233–4240 (7 2020). <https://doi.org/10.1109/LRA.2020.2993757>
- [14] Li, S., Duong, T.T.H., Zanotto, D.: In-flight cable length control for improved quadrotor-based suspended load transportation. IEEE Robotics and Automation Letters **9**(1), 667–674 (2024). <https://doi.org/10.1109/LRA.2023.3335778>
- [15] Loianno, G., Kumar, V.: Cooperative transportation using small quadrotors using monocular vision and inertial sensing. IEEE Robotics and Automation Letters **3**(2), 680–687 (4 2018). <https://doi.org/10.1109/LRA.2017.2778018>
- [16] Meng, J., Buzzatto, J., Liu, Y., Liarakapis, M.: On Aerial Robots with Grasping and Perching Capabilities: A Comprehensive Review. Front. Rob. AI **8**, 739173 (Mar 2022). <https://doi.org/10.3389/frobt.2021.739173>
- [17] Morin, D.G., Araujo, J., Tayamon, S., Andersson, L.A.A.: Autonomous Cooperative Flight of Rigidly Attached Quadcopters. In: 2019 International Conference on Robotics and Automation (ICRA). pp. 5309–5315 (2019). <https://doi.org/10.1109/ICRA.2019.8794266>
- [18] Mu, B., Chirarattananon, P.: Universal flying objects: Modular multirotor system for flight of rigid objects. IEEE Transactions on Robotics **36**(2), 458–471 (2020). <https://doi.org/10.1109/TRO.2019.2954679>
- [19] Oishi, K., Amano, Y., Jimbo, T.: Cooperative transportation using multiple single-rotor robots and decentralized control for unknown payloads. In: 2022 International Conference on Robotics and Automation (ICRA). pp. 2024–2030 (2022). <https://doi.org/10.1109/ICRA46639.2022.9811768>
- [20] Ollero, A., Tognon, M., Suarez, A., Lee, D., Franchi, A.: Past, Present, and Future of Aerial Robotic Manipulators. IEEE Transactions on Robotics **38**(1), 626–645 (2 2022). <https://doi.org/10.1109/TRO.2021.3084395>
- [21] Seth, A., James, A., Kuantama, E., Mukhopadhyay, S., Han, R.: Aerodynamics and sensing analysis for efficient drone-based parcel delivery. In: 2023 16th International Conference on Sensing Technology (ICST). pp. 1–6 (2023). <https://doi.org/10.1109/ICST59744.2023.10460847>
- [22] Seth, A., James, A., Kuantama, E., Mukhopadhyay, S., Han, R.: Drone High-Rise Aerial Delivery with Vertical Grid Screening. Drones **7**(5), 300 (May 2023). <https://doi.org/10.3390/drones7050300>
- [23] Villa, D.K.D., Brandao, A.S., Carelli, R., Sarcinelli-Filho, M.: Cooperative load transportation with two quadrotors using adaptive control. IEEE Access **9**, 129148–129160 (2021). <https://doi.org/10.1109/ACCESS.2021.3113466>
- [24] Webb, K., Rogers, J.: Adaptive control design for multi-uav cooperative lift systems. Journal of Aircraft **58**(6), 1302–1322 (7 2021). <https://doi.org/https://arc.aiaa.org/doi/10.2514/1.C036206>
- [25] Welde, J., Paulos, J., Kumar, V.: Dynamically feasible task space planning for underactuated aerial manipulators. IEEE Robotics and Automation Letters **6**(2), 3232–3239 (2021). <https://doi.org/10.1109/LRA.2021.3051572>
- [26] Zhao, M., Okada, K., Inaba, M.: Versatile articulated aerial robot DRAGON: Aerial manipulation and grasping by vectorable thrust control. International Journal of Robotics Research (2022). <https://doi.org/10.1177/02783649221112446>
- [27] Zhou, X., Wen, X., Wang, Z., Gao, Y., Li, H., Wang, Q., Yang, T., Lu, H., Cao, Y., Xu, C., Gao, F.: Swarm of micro flying robots in the wild. Science Robotics **7**(66) (May 2022). <https://doi.org/10.1126/scirobotics.abm5954>